frontiers | Frontiers in Physics

ORIGINAL RESEARCH
published: 26 May 2022
doi: 10.3389/fphy.2022.926344

Passively Q-Switched and Mode-Locked Fiber Laser Based on a Zeolitic Imidazolate Framework-67 Saturable Absorber

*Pengpeng Wang and Cunguang Zhu**

School of Physics Science and Information Technology, Liaocheng University, Liaocheng, China

Exploring new saturable absorber (SA) materials with excellent performance to achieve Q-switching and mode-locking operations is a hot topic in ultrafast laser research. The impressive specific surface areas, structural tunability, and high thermal and chemical stability of the zeolitic imidazolate framework (ZIF) materials make them promising candidates as high-performance SAs. In this work, we demonstrated the potential of the ZIF-67 SAs for ultrafast fiber laser applications. The nonlinear optical absorption characteristics of the ZIF-67 SAs at the telecommunication band were investigated by using the balanced twin-detector method. By incorporating the ZIF-67 SAs into the Er^{3+}-doped fiber laser cavity, stable Q-switching and mode-locking operations were achieved. The research results are essential for promoting the application of novel hybrid nanomaterials in ultrafast lasers.

Keywords: saturable absorber, mode-locking, Er^{3+}-doped fiber laser, ZIF, hybrid nanomaterials

OPEN ACCESS

Edited by:
Wenjing Tang,
University of Jinan, China

Reviewed by:
Huannian Zhang,
Shandong University of Technology, China
Tianli Feng,
Shandong University, China

****Correspondence:***
Cunguang Zhu
cunguang_zhu@163.com

Specialty section:
This article was submitted to Optics and Photonics, a section of the journal Frontiers in Physics

Received: *22 April 2022*
Accepted: *12 May 2022*
Published: *26 May 2022*

Citation:
Wang P and Zhu C (2022) Passively Q-Switched and Mode-Locked Fiber Laser Based on a Zeolitic Imidazolate Framework-67 Saturable Absorber. Front. Phys. 10:926344. doi: 10.3389/fphy.2022.926344

INTRODUCTION

As a typical representative of third-generation lasers, fiber lasers are promising in many scientific and industrial fields, occupying a large share of the commercial laser market. Fiber lasers can be divided into two types depending on the mode of operation: continuous and pulsed. The pulsed fiber laser has high pulse energy and short pulse width, greatly expanding the application of lasers in fiber optic communication, automotive manufacturing, laser cutting, medical devices, and other fields. Q-switching and mode-locking are the two main techniques enabling pulsed laser, both of which can be implemented actively or passively. The passive approach has gained increasing interest in the last few years due to its simplicity, flexibility, compactness, and low manufacturing cost. Unlike the active approach, the passive one does not rely on bulky and complex optical modulators and electronic drivers, which can achieve laser pulse output simply by placing a saturable absorber (SA) in the resonant cavity. Therefore, the SA plays a crucial role in the passive Q-switched and mode-locked lasers. The development of passive pulsed lasers relies heavily on SA materials.

Several types of SA materials have been investigated to realize passive pulsed lasers, such as transition metal dichalcogenides [1–8], topological insulators [9–13], carbon nanotubes [14, 15], graphene [16–19], transition metal oxide [20–23], black phosphorus [24–28], and ferromagnetic semiconductors [29]. In some recent studies, it has been found that lasers can perform both Q-switching and mode-locking operations with the help of some excellent SA materials. In 2018, D. Mao et al. successfully realized Q-switching and mode-locking operations using a film-type ReS_2-PVA SA in an erbium-doped fiber laser (EDFL) [30]. In 2019, C. Wei et al. reported the implementation of the Q-switching and mode-locking operations in a Ho^{3+}/Pr^{3+} co-doped ZBLAN fiber laser at 3 μm mid-infrared waveband using a single-walled carbon nanotube SA [31]. In 2020, N.F. Zulkiplia et al. achieved two modes of pulsed EDFLs using Eu_2O_3 as a SA [23]. In the

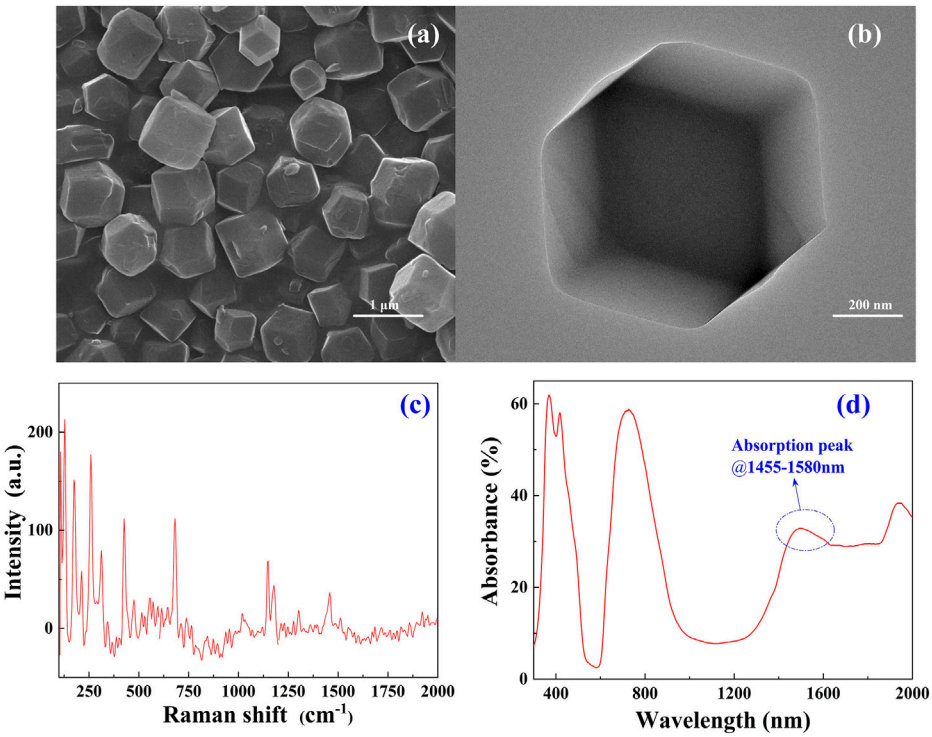

FIGURE 1 | Characteristics of the ZIF-67: **(A)** SEM image; **(B)** TEM image; **(C)** Raman spectrum; **(D)** Visible-NIR spectrum.

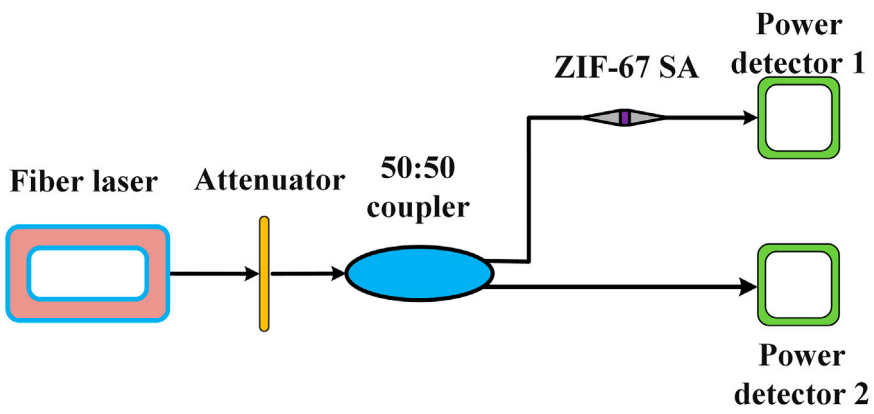

FIGURE 2 | The setup for determining the nonlinear optical absorption characteristics of the ZIF-67 SAs.

same year, W. Zhang et al. successfully built Q-switched and mode-locked erbium-doped fiber lasers using tellurene nanosheets as SAs [32]. It is of great interest to continue exploring new SA materials that can perform multiple types of pulsed operations.

Metal-organic frameworks (MOFs) have attracted a great deal of attention in the past decade. They are hybrid materials with repeating, cage-like structures constructed with metal/metal-cluster nodes bridged by organic linkers. With high internal surface areas and unique structure design and tunability, MOFs have proven to be excellent gas storage [33], gas sensors [34], supercapacitors [35], and catalysts [36]. MOFs can possess favorable photophysical properties due to the coordination of metal nodes with organic linkers [37, 38], making them one of the most promising materials for applications in nonlinear optics, especially in ultrafast lasers [39, 40]. However, the poor hydrothermal and chemical stability has limited the application of MOFs in some fields. Under high temperature, high humidity, or strong acidic and alkaline environments, the coordination bonds between metal ions and organic ligands in MOFs are easily broken, leading to framework changes or even collapse.

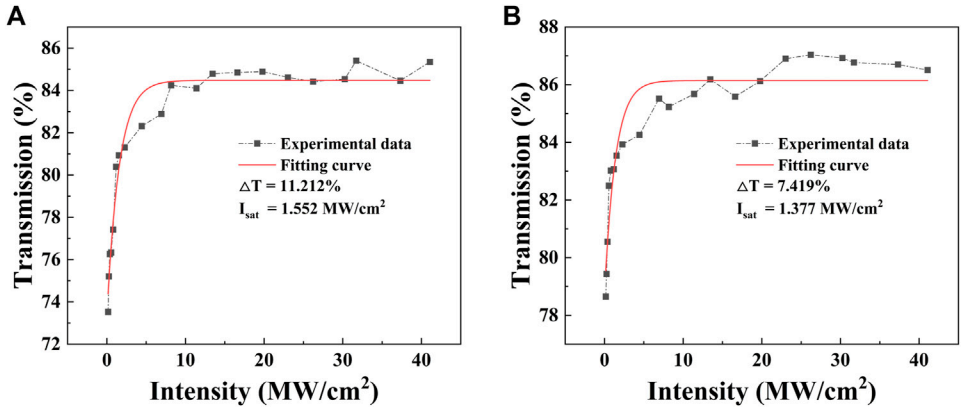

FIGURE 3 | The nonlinear optical absorption characteristics of **(A)** SA1 and **(B)** SA2.

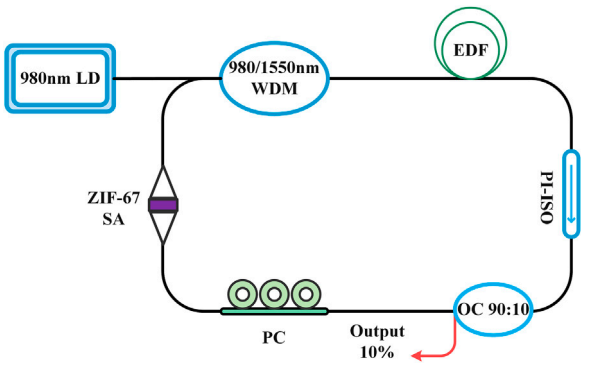

FIGURE 4 | Experimental schematic of the ZIF-67-based Er^{3+}-doped fiber laser.

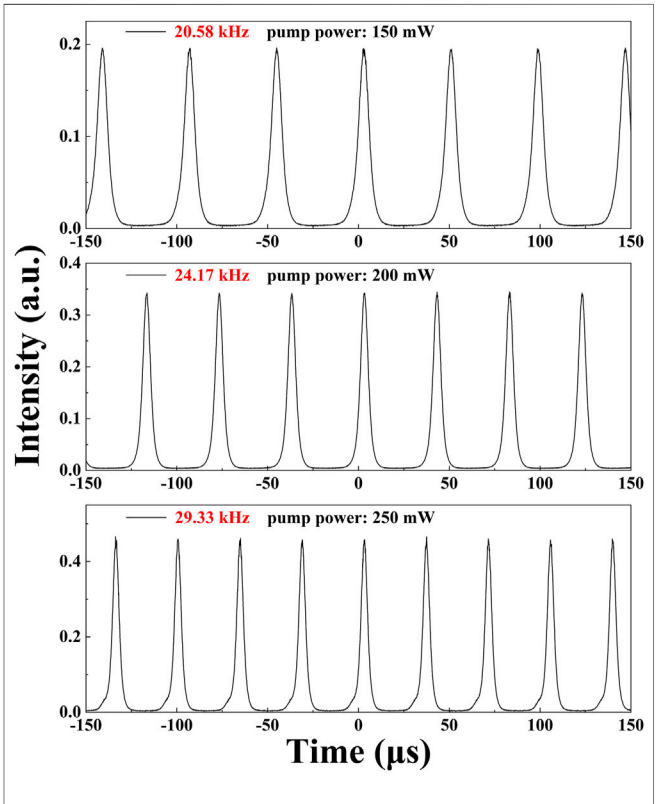

FIGURE 5 | The typical oscilloscope traces of the Q-switched pulse trains under different pump power.

Exploring a new material that exhibits better hydrothermal and chemical stability and inherits the advantages of MOFs is a good option to solve the above problems. As a subfamily of MOFs, zeolitic imidazolate framework (ZIF) materials have all these qualities [41, 42]. They are porous materials consisting of transition metal ions cobalt (Co^{2+}) or zinc (Zn^{2+}) bonded by imidazole. In recent years, H. Chu et al. first investigated the nonlinear saturable absorption properties of ZIF-67 materials in the near- and mid-infrared spectral bands and designed passive Q-switched solid-state lasers based on ZIF-67 SAs operating at 1, 1.3, 2, and 2.3 μm wavelength, respectively [43–46]. These results fully illustrate the excellent nonlinear saturable absorption properties of the ZIF-67 materials. However, up to now, the research reports based on ZIF-67 are limited to solid-state lasers, and only passive Q-switching operation has been achieved. The nature and applications of ZIFs in ultrafast lasers are to be further explored.

This work demonstrated the potential of ZIF-67 SAs for ultrafast fiber laser applications. By incorporating the ZIF-67 SAs into the Er^{3+}-doped fiber laser cavity, stable Q-switching and mode-locking operations were achieved. To the best of our knowledge, it is the first time ZIF-67 has been implemented as SAs in a fiber laser for both Q-switching and mode-locking operations.

FABRICATION AND CHARACTERIZATION OF ZEOLITIC IMIDAZOLATE FRAMEWORK-67 SATURABLE ABSORBERS

We initially fabricated fiber-compatible ZIF-67 SAs to integrate the ZIF-67 materials into a fiber laser cavity. The fabrication process follows: First, bulk-state ZIF-67 crystals were ground into

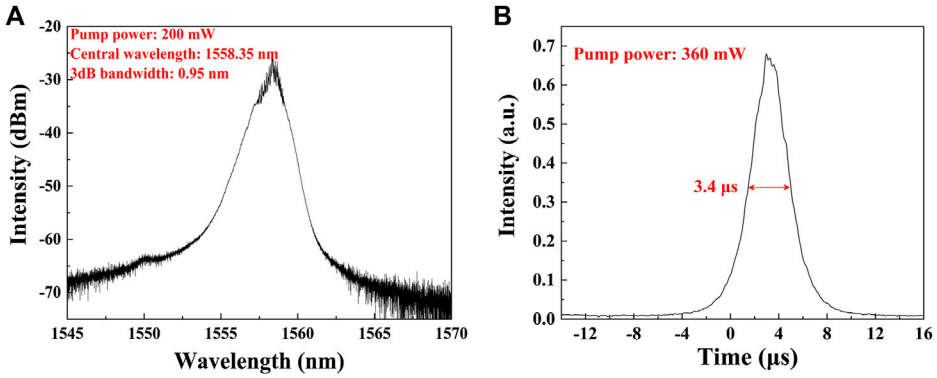

FIGURE 6 | (A) The optical spectrum; **(B)** A single-pulse profile of the Q-switched pulses.

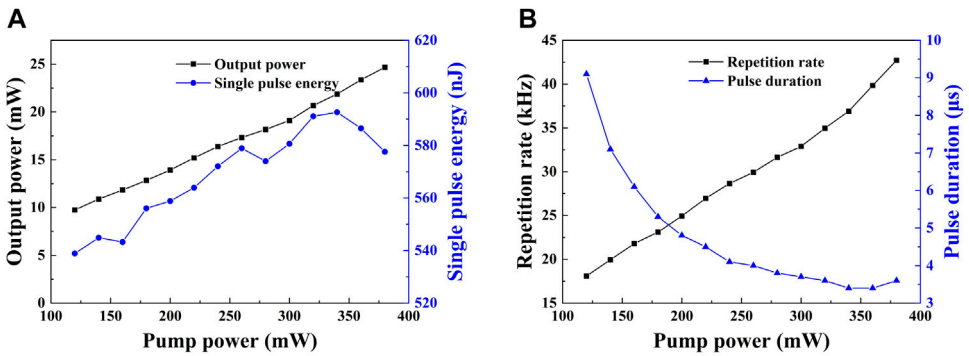

FIGURE 7 | The evolution of **(A)** average output power and single pulse energy, **(B)** repetition rate and pulse duration as pump power increase.

powder in a ball mill. Second, 2 g purple ZIF-67 powder dispersed in 50 ml absolute ethanol solution was stirred with magnetic force at a rate of 1,500 rpm for 2 h. Third, the resulting mixture was placed in an ultrasonic cleaner for 8 h and then put into a centrifuge to remove the large sediment by high-speed centrifugation. The mixture was allowed to stand for 12 h, and the supernatant was then taken for SAs preparation. In the final step, we dropped the ZIF-67 dispersion onto the fiber connector end facet with a dropper and placed it vertically downward until it dried naturally. After repeating this step several times, about 50–100 μl of ZIF-67 dispersion was coated onto the fiber connector end facet. A fiber-compatible ZIF-67 SA was finally obtained by connecting a dispersion-coated fiber connector to a clean fiber connector with a fiber optic adapter.

The surface morphology of the as-prepared ZIF-67 crystals was investigated by SEM (Quanta FEG 250, FEI) and TEM (JEM-2100F, JEOL). The SEM and TEM images show that the as-prepared ZIF-67 materials possess a rhombic dodecahedral morphology with uniform particle size distribution. The particle size is about 500 nm. The structural characterization of the ZIF-67 materials was determined by Raman spectroscopy with a spectral resolution of 2 cm^{-1}, recorded by a Raman spectrometer under 633 nm laser excitation. The distinct vibrational modes observed in **Figure 1C** generally agree with the previous research description. **Figure 1D** illustrates the spectral absorbance of the ZIF-67 materials in the visible and near-infrared bands, revealing an absorption peak in the band from 1,455 nm to 1,580 nm.

We further investigated the nonlinear optical absorption characteristics of the ZIF-67 SAs by using the balanced twin-detector method. The test setup is shown in **Figure 2**. A homemade nonlinear polarization rotation (NPR) EDFL with a pulse width of ~643 fs at 1575.62 nm and a repetition rate of 26.04 MHz was employed as the probe light source. The transmittance at different incident light intensities was fitted by the following equation:

$$T = 1 - \Delta T \exp\left(-\frac{I}{I_{sat}}\right) - T_{ns}, \quad (1)$$

where T is the transmittance, ΔT is the modulation depth, I is the incident intensity, I_{sat} is the saturation intensity and T_{ns} is the non-saturable loss.

We tested two as-fabricated ZIF-67 SAs successively, and the tested results and the fitting curves are shown in **Figure 3**. According to the fitting curve in **Figure 3A**, the saturation intensity, modulation depth, and non-saturable loss of the first

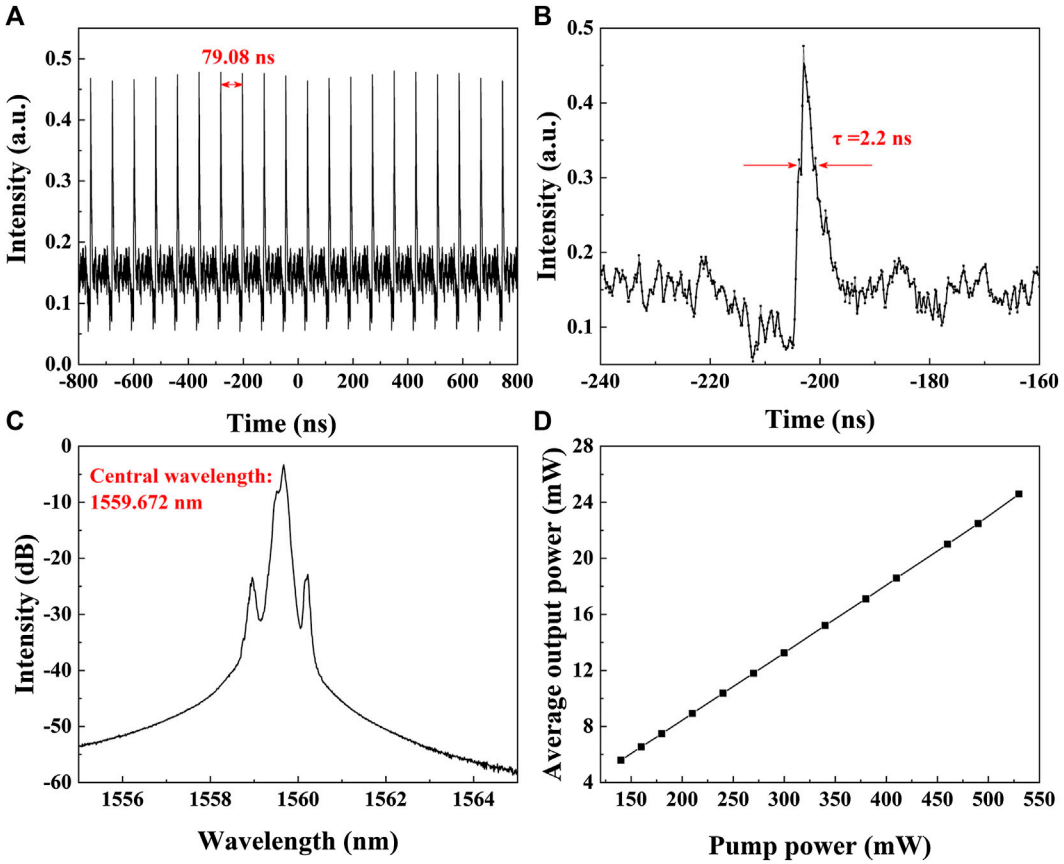

FIGURE 8 | Mode-locking performance: **(A)** Oscilloscope trace of the pulse train; **(B)** Oscilloscope trace of a single pulse; **(C)** Optical spectrum; **(D)** Output power versus pump power.

ZIF-67 SA (referred to as SA1 later) are approximately 1.552 MW/cm^2, 11.212%, and 15.523%, respectively, which has been used in **Section 4.1** to reveal the Q-switching ability of the ZIF-67 SAs. As shown in **Figure 3B**, the other ZIF-67 SA (referred to as SA2 later) features a saturation intensity of 1.377 MW/cm^2, a modulation depth of 7.419%, and a non-saturable loss of 13.858%, which has been used in **Section 4.2** to initiate the mode-locking operation.

EXPERIMENTAL SETUP

Figure 4 shows the experimental setup of the pulsed Er^{3+}-doped fiber laser incorporating the fabricated ZIF-67 SAs. The pump energy from a 980-nm band laser diode (LD) pump source with a maximum output power of 600 mW was guided into the laser cavity by a 980/1,550 nm wavelength division multiplexer (WDM). A 60 cm long Er^{3+}-doped fiber (EDF, Liekki Er-80, 8/125) was served as the laser gain medium with a dispersion parameter of ~15.7 ps/nm/km. The Er^{3+} concentration and nominal absorption at 1,530 nm were 3,150 ppm and 80 dB/m, respectively. A polarization-insensitive isolator (PI-ISO) ensured unidirectional propagation of light in the cavity. A polarization controller (PC) was used to adjust the polarization state and birefringence in the cavity. The ZIF-67 SAs were inserted between the WDM and PC. The laser output from the 10% port of a 90:10 optical coupler (OC). The temporal characteristics of the output laser were recorded by a 3 GHz fast speed PIN photodetector combined with a digital oscilloscope (MDO3102, Tektronix). The optical spectral characteristics of the output laser were measured by an optical spectrum analyzer (AQ6370, Yokogawa). The radio-frequency (RF) spectrum was analyzed by a spectrum analyzer (FPC1000, Rohde & Schwarz). The output power was monitored by an optical power meter.

EXPERIMENTAL RESULTS AND DISCUSSIONS

Q-Switching Performance

To exclude the possibility of the self-Q-switching or self-mode-locking operation in the EDFL without the ZIF-67 SA, we did not insert the SA into the laser cavity at first. Only continuous-wave operation was observed during the adjustment of the pump power or the PC. Instead, once the ZIF-67 SA1 was inserted into the laser cavity, the remarkable passively Q-switched pulse

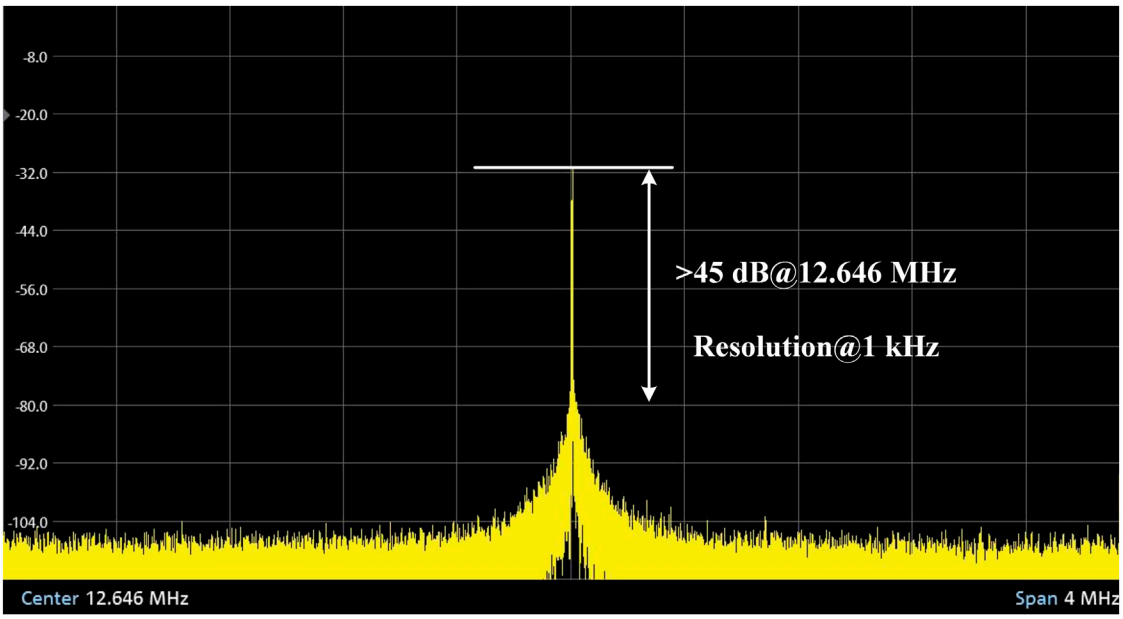

FIGURE 9 | RF spectrum at a fundamental frequency of 12.646 MHz with 1 kHz resolution. The unit of the vertical axis is dBm.

trains can be observed when the pump power exceeded 108 mW. The typical oscilloscope traces of the Q-switched pulse trains under different pump power are shown in **Figure 5**. As the pump power varied from 150 to 250 mW, the pulse output stayed stable, and the repetition rates were increased from 20.58 to 29.33 kHz. As commonly observed in passively Q-switched lasers, the pulse repetition rate increases, and the pulse width becomes narrower as the pump power increases.

The corresponding optical spectrum is shown in **Figure 6A**. The laser wavelength is centered at 1558.35 nm with a 3-dB bandwidth of 0.95 nm. **Figure 6B** shows a single-pulse profile of the Q-switched pulses at the pump power of 360 mW and exhibits that the pulse duration is 3.4 μs? The corresponding pulse repetition rate is 39.84 kHz, shown in **Figure 7B**. Both the pulse duration and spectral width agree with the typical feature of Q-switched fiber lasers. Varying the polarization state in the cavity hardly changes the characteristics of the pulse trains and the optical spectrum, indicating that the fiber laser's Q-switching operation is polarization insensitive.

The characteristics of the laser pulses as a function of pump power are shown in **Figure 7**. **Figure 7A** shows the dependence of the average output power and the single pulse energy on the pump power, and **Figure 7B** shows the pulse duration and the pulse repetition rate versus the pump power. As the pump power increased from 120 to 360 mW, the Q-switching operation remained stable. The average output power increased almost linearly with the pump power, from 9.75 to 24.67 mW. The single pulse energy can reach up to 592.59 nJ. The pulse duration gradually decreased from 9.1 to 3.4 μs? However, when the pump power reached 380 mW, the pulses turned unstable, and the top of the pulse tended to split. The pulse width was slightly widened to 3.6 μs, resulting in a decrease in the single pulse energy to 577.59 nJ. Unlike the mode-locking operation, the generation of Q-switched pulses relies on the saturation of SA, which causes the repetition rate of the pulses to depend on the pump power rather than the cavity length. As shown in **Figure 7B**, the repetition rate is positively correlated with the pump power. The repetition rate increases from 18.08 to 42.71 kHz along with the increase of pump power from 120 to 360 mW. The reason is that the SA will saturate faster when increasing the pump power, which leads to an increase in repetition rate.

Mode-Locking Performance

Then, we inserted the other ZIF-67 SA (SA2) with an additional ~8 m of single-mode fiber (SMF) into the cavity. The dispersion parameter of the SMF is ~17 ps/nm/km. The total length of the cavity is about 16.25 m. Thus, the net dispersion of the Er^{3+}-doped fiber laser is calculated to be −0.35 ps^2.

After carefully adjusting the PC in the cavity, a stable self-started mode-locking operation was achieved when the pump power reached 90 mW. Limited by the maximum nominal power of 600 mW, the pump power was adjusted in the range of 90–530 mW, and the mode-locking operation can be maintained stable.

The mode-locking performance at the pump power of 410 mW is shown in **Figure 8**. A typical mode-locked pulse train with a pulse-to-pulse interval of 79.08 ns is shown in **Figure 8A**, corresponding to a fundamental repetition rate of 12.646 MHz with a total laser cavity length of ~16.25 m. The oscilloscope trace of a single mode-locked pulse is shown in **Figure 8B**. Due to the limitations of the response times of the detector and oscilloscope, the actual pulse duration is

undoubtedly shorter than the bandwidth of 2.2 ns recorded by the oscilloscope. The optical spectrum with a central wavelength of 1559.672 nm and a resolution bandwidth of 0.02 nm is shown in **Figure 8C**, where a typical Kelley sideband peak can be observed. **Figure 8D** shows the relationship between the average output power and the pump power, and it is clear that the output power is linearly related to the pump power. The maximum average output power was 24.58 mW under a pump power of 530 mW. As shown in **Figure 9**, the RF spectrum with a bandwidth of 4 MHz and a resolution of 1 kHz depicts the stability of the mode-locked laser with the fundamental repetition rate of 12.646 MHz. Continuous 4-h observation of the oscilloscope traces and optical spectra of the mode-locked pulses was performed to verify the long-term stability of the fiber laser. The pulse train and the central wavelength of the spectrum were always stable. After we stopped the laser for 24 h and turned the pump on again, the mode-locked pulse was still outputting stably, and the laser center wavelength was still stable at 1559.6 nm, which illustrates the long-term stability of the laser.

CONCLUSION

In this paper, the nonlinear optical absorption characteristics of the ZIF-67 SAs were discovered and investigated. The two fabricated ZIF-67 SAs with the modulation depth of 11.212% and 7.419% were subsequently used to implement stable Q-switching and mode-locking operations, respectively. Self-started Q-switched pulses at 1558.35 nm can be observed with a threshold pump power of 108 mW. The Q-switched pulse train remained stable as the pump power increased from 120 to 360 mW. The maximum single pulse energy can reach up to 592.59 nJ. The top of the pulse started to split until the pump power rose to 380 mW, resulting in a slight decrease in the single pulse energy and an increase in pulse duration. In the mode-locking operation, a typical mode-locked pulse train with a pulse-to-pulse interval of 79.08 ns and a central wavelength of 1559.672 nm was recorded with a total laser cavity length of ~16.25 m. The typical Kelley sideband peak can also be observed. These results demonstrate that the ZIF-67-based SA can serve as a promising mode locker and Q-switcher in the field of ultrafast lasers.

DATA AVAILABILITY STATEMENT

The original contributions presented in the study are included in the article/supplementary material, further inquiries can be directed to the corresponding author.

AUTHOR CONTRIBUTIONS

PW: conceptualization, methodology, original draft preparation. CZ: reviewing and editing.

FUNDING

This work is supported by National Natural Science Foundation of China (61705080); Promotive Research Fund for Excellent Young and Middle-aged Scientists of Shandong Province (ZR2016FB17, BS2015DX005); Scientific Research Foundation of Liaocheng University (318012101); Startup Foundation for Advanced Talents of Liaocheng University (318052156, 318052157).

REFERENCES

1. Li L, Pang L, Wang Y, Liu W. WxNb(1−x)Se2 Nanosheets for Ultrafast Photonics. *Nanoscale* (2021) 13:2511–8. doi:10.1039/d0nr08580d
2. Li L, Pang L, Zhao Q, Liu W, Su Y. VSe2 Nanosheets for Ultrafast Fiber Lasers. *J Mater Chem C* (2020) 8:1104–9. doi:10.1039/c9tc06159b
3. Chen B, Zhang X, Wu K, Wang H, Wang J, Chen J. Q-switched Fiber Laser Based on Transition Metal Dichalcogenides MoS_2, MoSe_2, WS_2, and WSe_2. *Opt Express* (2015) 23:26723. doi:10.1364/oe.23.026723
4. Niu K, Sun R, Chen Q, Man B, Zhang H. Passively Mode-Locked Er-Doped Fiber Laser Based on SnS_2 Nanosheets as a Saturable Absorber. *Photon Res* (2018) 6:72. doi:10.1364/prj.6.000072
5. Ming N, Tao S, Yang W, Chen Q, Sun R, Wang C, et al. Mode-locked Er-Doped Fiber Laser Based on PbS/CdS Core/shell Quantum Dots as Saturable Absorber. *Opt Express* (2018) 26:9017. doi:10.1364/oe.26.009017
6. Shang X, Guo L, Zhang H, Li D, Yue Q. Titanium Disulfide Based Saturable Absorber for Generating Passively Mode-Locked and Q-Switched Ultra-fast Fiber Lasers. *Nanomaterials* (2020) 10:1922. doi:10.3390/nano10101922
7. Xu N, Wang H, Zhang H, Guo L, Shang X, Jiang S, et al. Palladium Diselenide as a Direct Absorption Saturable Absorber for Ultrafast Mode-Locked Operations: from All Anomalous Dispersion to All normal Dispersion. *Nanophotonics* (2020) 9:4295–306. doi:10.1515/nanoph-2020-0267
8. Shang X, Xu N, Zhang H, Li D. Nonlinear Photoresponse of High Damage Threshold Titanium Disulfide Nanocrystals for Q-Switched Pulse Generation. *Opt Laser Tech* (2022) 151:107988. doi:10.1016/j.optlastec.2022.107988
9. Xu N, Ming N, Han X, Man B, Zhang H. Large-energy Passively Q-Switched Er-Doped Fiber Laser Based on CVD-Bi2Se3 as Saturable Absorber. *Opt Mater Express* (2019) 9:373. doi:10.1364/ome.9.000373
10. Guo Q, Pan J, Liu Y, Si H, Lu Z, Han X, et al. Output Energy Enhancement in a Mode-Locked Er-Doped Fiber Laser Using CVD-Bi2Se3 as a Saturable Absorber. *Opt Express* (2019) 27:24670. doi:10.1364/oe.27.024670
11. Guo B, Yao Y, Yang Y-F, Yuan Y-J, Jin L, Yan B, et al. Dual-wavelength Rectangular Pulse Erbium-Doped Fiber Laser Based on Topological Insulator Saturable Absorber. *Photon Res* (2015) 3:94. doi:10.1364/prj.3.000094
12. Liu H, Zheng X-W, Liu M, Zhao N, Luo A-P, Luo Z-C, et al. Femtosecond Pulse Generation from a Topological Insulator Mode-Locked Fiber Laser. *Opt Express* (2014) 22:6868. doi:10.1364/oe.22.006868
13. Luo Z-C, Liu M, Liu H, Zheng X-W, Luo A-P, Zhao C-J, et al. 2 GHz Passively Harmonic Mode-Locked Fiber Laser by a Microfiber-Based Topological Insulator Saturable Absorber. *Opt Lett* (2013) 38:5212. doi:10.1364/ol.38.005212
14. Wei C, Zhang H, Kang Z, Qin G, Liu Y. Wideband Tunable Passively Q-Switched Fiber Laser at 28 μm Using a Broadband Carbon Nanotube Saturable Absorber. *Photon Res* (2019) 7:14.
15. Li W, Zhu C, Rong X, Wu J, Xu H, Wang F, et al. Bidirectional Red-Light Passively Q-Switched All-Fiber Ring Lasers with Carbon Nanotube Saturable Absorber. *J Lightwave Technol* (2018) 36:2694–701. doi:10.1109/jlt.2017.2781702
16. Popa D, Sun Z, Torrisi F, Hasan T, Wang F, Ferrari AC. Sub 200 Fs Pulse Generation from a Graphene Mode-Locked Fiber Laser. *Appl Phys Lett* (2010) 97:203106. doi:10.1063/1.3517251

17. Sulimany K, Lib O, Masri G, Klein A, Fridman M, Grelu P, et al. Bidirectional Soliton Rain Dynamics Induced by Casimir-like Interactions in a Graphene Mode-Locked Fiber Laser. *Phys Rev Lett* (2018) 121:133902. doi:10.1103/physrevlett.121.133902
18. Zhang H, Tang D, Knize RJ, Zhao L, Bao Q, Loh KP. Graphene Mode Locked, Wavelength-Tunable, Dissipative Soliton Fiber Laser. *Appl Phys Lett* (2010) 96:111112. doi:10.1063/1.3367743
19. Wang ZT, Chen Y, Zhao CJ, Zhang H, Wen SC. Switchable Dual-Wavelength Synchronously Q-Switched Erbium-Doped Fiber Laser Based on Graphene Saturable Absorber. *IEEE Photon J.* (2012) 4:869–76. doi:10.1109/jphot.2012.2199102
20. Bai X, Mou C, Xu L, Wang S, Pu S, Zeng X. Passively Q-Switched Erbium-Doped Fiber Laser Using Fe3O4-Nanoparticle Saturable Absorber. *Appl Phys Express* (2016) 9:042701. doi:10.7567/apex.9.042701
21. Wang P, Zhu C, Sun Y, Zhao Y. Mode-locked Fiber Laser Based on α-Fe2O3 Nanosheets as Saturable Absorbers. *Opt Laser Tech* (2021) 144:107417. doi:10.1016/j.optlastec.2021.107417
22. Khaleel WA, Sadeq SA, Alani IAM, Ahmed MHM. Magnesium Oxide (MgO) Thin Film as Saturable Absorber for Passively Mode Locked Erbium-Doped Fiber Laser. *Opt Laser Tech* (2019) 115:331–6. doi:10.1016/j.optlastec.2019.02.042
23. Zulkipli NF, Jafry AAA, Apsari R, Samsamnun FSM, Batumalay M, Khudus MIMA, et al. Generation of Q-Switched and Mode-Locked Pulses with Eu_2O_3 Saturable Absorber. *Opt Laser Tech* (2020) 127:106163. doi:10.1016/j.optlastec.2020.106163
24. Luo Z-C, Liu M, Guo Z-N, Jiang X-F, Luo A-P, Zhao C-J, et al. Microfiber-based Few-Layer Black Phosphorus Saturable Absorber for Ultra-fast Fiber Laser. *Opt Express* (2015) 23:20030. doi:10.1364/oe.23.020030
25. Sotor J, Sobon G, Macherzynski W, Paletko P, Abramski KM. Black Phosphorus Saturable Absorber for Ultrashort Pulse Generation. *Appl Phys Lett* (2015) 107:051108. doi:10.1063/1.4927673
26. Qin Z, Xie G, Zhang H, Zhao C, Yuan P, Wen S, et al. Black Phosphorus as Saturable Absorber for the Q-Switched Er:ZBLAN Fiber Laser at 28 μm. *Opt Express* (2015) 23:24713. doi:10.1364/oe.23.024713
27. Wang J, Xing Y, Chen L, Li S, Jia H, Zhu J, et al. Passively Q-Switched Yb-Doped All-Fiber Laser with a Black Phosphorus Saturable Absorber. *J Lightwave Tech* (20182010–2016) 36. doi:10.1109/jlt.2018.2800910
28. Zhang M, Wu Q, Zhang F, Chen L, Jin X, Hu Y, et al. 2D Black Phosphorus Saturable Absorbers for Ultrafast Photonics. *Adv Opt Mater* (2019) 7:1800224. doi:10.1002/adom.201800224
29. Xu N, Sun S, Shang X, Zhang H, Li D. Harmonic and Fundamental-Frequency Mode-Locked Operations in an Er-Doped Fiber Laser Using a Cr2Si2Te6-Based Saturable Absorber. *Opt Mater Express* (2022) 12:166–73. doi:10.1364/ome.446815
30. Mao D, Cui X, Gan X, Li M, Zhang W, Lu H, et al. Passively Q-Switched and Mode-Locked Fiber Laser Based on an ReS2 Saturable Absorber. *IEEE J Select Top Quan Electron.* (2018) 24:1–6. doi:10.1109/jstqe.2017.2713641
31. Wei C, Lyu Y, Shi H, Kang Z, Zhang H, Qin G, et al. Mid-Infrared Q-Switched and Mode-Locked Fiber Lasers at 2.87 μm Based on Carbon Nanotube. *IEEE J Select Top Quan Electron.* (2019) 25:1–6. doi:10.1109/jstqe.2019.2899015
32. Zhang W, Wang G, Xing F, Man Z, Zhang F, Han K, et al. Passively Q-Switched and Mode-Locked Erbium-Doped Fiber Lasers Based on Tellurene Nanosheets as Saturable Absorber. *Opt Express* (2020) 28:14729. doi:10.1364/oe.392944
33. Sung Cho H, Deng H, Miyasaka K, Dong Z, Cho M, Neimark AV, et al. Extra Adsorption and Adsorbate Superlattice Formation in Metal-Organic Frameworks. *Nature* (2015) 527:503–7. doi:10.1038/nature15734
34. Wang X, Zhang S, Shao M, Huang J, Deng X, Hou P, et al. Fabrication of ZnO/ZnFe2O4 Hollow Nanocages through Metal Organic Frameworks Route with Enhanced Gas Sensing Properties. *Sensors Actuators B: Chem* (2017) 251:27–33. doi:10.1016/j.snb.2017.04.114
35. Salunkhe RR, Kaneti YV, Yamauchi Y. Metal-Organic Framework-Derived Nanoporous Metal Oxides toward Supercapacitor Applications: Progress and Prospects. *ACS Nano* (2017) 11:5293–308. doi:10.1021/acsnano.7b02796
36. Liang J, Liang Z, Zou R, Zhao Y. Heterogeneous Catalysis in Zeolites, Mesoporous Silica, and Metal-Organic Frameworks. *Adv Mater* (2017) 29:1701139. doi:10.1002/adma.201701139
37. Wei Z, Gu Z-Y, Arvapally RK, Chen Y-P, McDougald RN, Ivy JF, et al. Rigidifying Fluorescent Linkers by Metal-Organic Framework Formation for Fluorescence Blue Shift and Quantum Yield Enhancement. *J Am Chem Soc* (2014) 136:8269–76. doi:10.1021/ja5006866
38. Jiang X, Zhang L, Liu S, Zhang Y, He Z, Li W, et al. Ultrathin Metal-Organic Framework: An Emerging Broadband Nonlinear Optical Material for Ultrafast Photonics. *Adv Opt Mater* (2018) 6:1800561. doi:10.1002/adom.201800561
39. Mingabudinova LR, Vinogradov VV, Milichko VA, Hey-Hawkins E, Vinogradov AV. Metal-organic Frameworks as Competitive Materials for Non-linear Optics. *Chem Soc Rev* (2016) 45:5408–31. doi:10.1039/c6cs00395h
40. Qian J, Sun F, Qin L. Hydrothermal Synthesis of Zeolitic Imidazolate Framework-67 (ZIF-67) Nanocrystals. *Mater Lett* (2012) 82:220–3. doi:10.1016/j.matlet.2012.05.077
41. Zhong G, Liu D, Zhang J. The Application of ZIF-67 and its Derivatives: Adsorption, Separation, Electrochemistry and Catalysts. *J Mater Chem A* (2018) 6:1887–99. doi:10.1039/c7ta08268a
42. Krokidas P, Castier M, Moncho S, Sredojevic DN, Brothers EN, Kwon HT, et al. ZIF-67 Framework: A Promising New Candidate for Propylene/Propane Separation. Experimental Data and Molecular Simulations. *J Phys Chem C* (2016) 120:8116–24. doi:10.1021/acs.jpcc.6b00305
43. Pan H, Wang X, Chu H, Li Y, Zhao S, Li G, et al. Optical Modulation Characteristics of Zeolitic Imidazolate Framework-67 (ZIF-67) in the Near Infrared Regime. *Opt Lett* (2019) 44:5892. doi:10.1364/ol.44.005892
44. Pan H, Chu H, Wang X, Li Y, Zhao S, Li G, et al. Nonlinear Optical Features of Zeolitic Imidazolate Framework-67 Nanocrystals for Mid-infrared Pulse Generation. *Cryst Growth Des* (2020) 20:6683–90. doi:10.1021/acs.cgd.0c00842
45. Pan H, Chu H, Wang X, Li Y, Zhao S, Li G, et al. Optical Nonlinearity of Zeolitic Imidazolate Framework-67 in the Near-Infrared Region. *Mater Chem Front* (2020) 4:2081–8. doi:10.1039/d0qm00226g
46. Chu H, Dong L, Pan Z, Ma X, Zhao S, Li D. Passively Q-Switched Tm:YAP Laser with a Zeolitic Imidalate Framework-67 Saturable Absorber Operating at 3H4→3H5 Transition. *Opt Laser Tech* (2022) 147:107679. doi:10.1016/j.optlastec.2021.107679

Conflict of Interest: The authors declare that the research was conducted in the absence of any commercial or financial relationships that could be construed as a potential conflict of interest.

Publisher's Note: All claims expressed in this article are solely those of the authors and do not necessarily represent those of their affiliated organizations, or those of the publisher, the editors and the reviewers. Any product that may be evaluated in this article, or claim that may be made by its manufacturer, is not guaranteed or endorsed by the publisher.